Journal of Materials Chemistry

Cite this: *J. Mater. Chem.*, 2011, **21**, 12969

www.rsc.org/materials

PAPER

Deep-blue and white organic light-emitting diodes based on novel fluorene-cored derivatives with naphthylanthracene endcaps

Ting Zhang,[a] Di Liu,[b] Qian Wang,[b] Renjie Wang,[a] Huicai Ren[b] and Jiuyan Li*[a]

Received 6th April 2011, Accepted 12th June 2011
DOI: 10.1039/c1jm11438g

Novel fluorene based deep-blue-emitting molecules with naphthylanthracene endcaps, namely 2,7-di(10-naphthylanthracene-9-yl)-9,9-dioctylfluorene (**NAF1**) and 7,7′-di(10-naphthylanthracene-9-yl)-9,9,9′,9′-tetraoctyl-2,2′-bifluorene (**NAF2**), are synthesized by a Suzuki cross-coupling reaction. These materials exhibit excellent thermal and amorphous stabilities, and high fluorescence quantum yield of over 70%. Organic light-emitting devices (OLEDs) using **NAF1** or **NAF2** as non-doped emitter exhibit bright deep blue electroluminescence with CIE coordinates of (0.15, 0.13) for **NAF1**, (0.16, 0.13) for **NAF2**. A maximum power efficiency of 2.2 lm W^{-1} (4.04 cd A^{-1}, 4.04%) is achieved for **NAF1**, which is among the highest values ever reported for deep-blue fluorescent OLEDs. A further improved coordinates of (0.15, 0.09) with efficiencies of 3.56 cd A^{-1} and 2.10 lm W^{-1} are achieved for **NAF1** upon tuning device thickness, which are also among the best data for non-doped deep blue fluorescent OLEDs with a CIE coordinate of $y < 0.1$. **NAF1** serves as excellent host emitter when doped with an orange fluorophore (4-(dicyanomethylene)-2-*tert*-butyl-6-(1,1,7,7-tetramethyljulolidyl-9-enyl)-4*H*-pyran, DCJTB). Upon careful tuning the doping level, the two-emitting-component (**NAF1** : DCJTB) OLED realizes efficient white light emission with a power efficiency of 3.01 lm W^{-1} (7.66 cd A^{-1}), a brightness of 12090 cd m^{-2}, and a standard white light coordinates of (0.33, 0.33). This performance is among the best results ever reported for two-emitting-component white OLEDs based on fluorescent materials.

Introduction

Organic light-emitting diodes (OLEDs) have attracted more and more research attention because of their promising applications in full-color, large-area flat-panel displays and solid-state lighting.[1,2] Compared with green-emitting materials, blue-emitting materials still have some problems such as imbalance of carrier transporting, low efficiency and especially poor color purity.[3–5] In recent years, great efforts have been taken to tune the color of blue electroluminescence (EL) into the deep blue region with a Commisssion Internationale de L'Eclairage (CIE) coordinate value of $y < 0.1$. Charge-transporting emitters and their non-doped OLEDs are apparently advantageous in terms of ease of device fabrication, low cost especially in mass production, and absence of phase separation or spectra shift with driving voltage. Among the three primary color emitting materials, blue host emitters are especially more significant than other two color ones, since otherwise a purple-light-emitting host material having larger band gap would be necessary for efficient energy transfer to a blue dopant. However, the large-band-gap host materials are relatively rare and always keep as one of the most challenging targets of OLED research. Fortunately, more and more blue fluorescent host emitters have been developed to fabricate non-doped deep blue OLEDs with CIE coordinate value of $y < 0.15$ or even < 0.1.[6,7]

Due to the relatively large band gaps, the blue host emitting materials are additionally valuable to serve as the matrix emitters for low-energy dopants to fabricate other single-color and even white OLEDs.[8–11] White OLEDs are of special interests in both research and industry fields due to their practical application as new-generation lighting source and backlight of flat-panel displays.[12,13] In general, white OLEDs can be obtained by incorporating either three primary colors (red, green, and blue) or two complementary color ones (blue and yellow or orange) in a multi- or a single-layer structure. Due to the simplicity of device structure and fabricating process and the excellent device performance, the two-emitting-component strategy has ascended to be one important method for fabrication of WOLEDs.[14–16] In this type of white OLEDs, the proper doping level and thus the extent of energy transfer from the blue host to the orange dopant are the key points to control the color purity of white light. In addition, the luminescent efficiencies of both the blue host and the orange dopant are essential to determine

[a]*State Key Laboratory of Fine Chemicals, School of Chemical Engineering, Dalian University of Technology, 2 Linggong Road, Dalian, 116024, China. E-mail: jiuyanli@dlut.edu.cn; Fax: +86 411 84986233*
[b]*School of Chemistry, Dalian University of Technology, 2 Linggong Road, Dalian, 116024, China*

the overall efficiency of white light. Therefore, excellent blue host emitters are sought for white OLEDs application. Recently a few blue fluorophores were successfully used to fabricate white OLEDs. For example, Shu *et al.* reported that an anthracene derivative end-capped with tetraphenylethylene groups, namely TPVAn, exhibited an efficiency of 5.3 cd A^{-1} with CIE coordinates of (0.14, 0.12) in its non-doped blue OLED, and the two-component white OLED containing TPVAn as blue host and an orange fluorescent dopant realized a high efficiency of 4.9% with CIE coordinates of (0.33, 0.39). Both these blue and white OLEDs performances are among the best data for fluorescent materials.[17]

In this paper, we report the synthesis and luminescent properties of a group of novel fluorene-based deep blue emitters with naphthylanthracene endcaps, namely **NAF1** and **NAF2** (Scheme 1). Anthracene[18] and fluorene[19] are important building blocks to construct blue luminescent dyes due to their merits such as high fluorescent quantum yield, wide band gap and ease to be modified. However, neither of them exhibits good color purity nor stable thermal stability in organic light-emitting devices since both of them are easy to recrystallize and have low glass transition temperature. This situation didn't change until the appearance of oligomer light-emitting materials such as oligofluorenes.[20] Herein, we select the oligofluorene as the core and

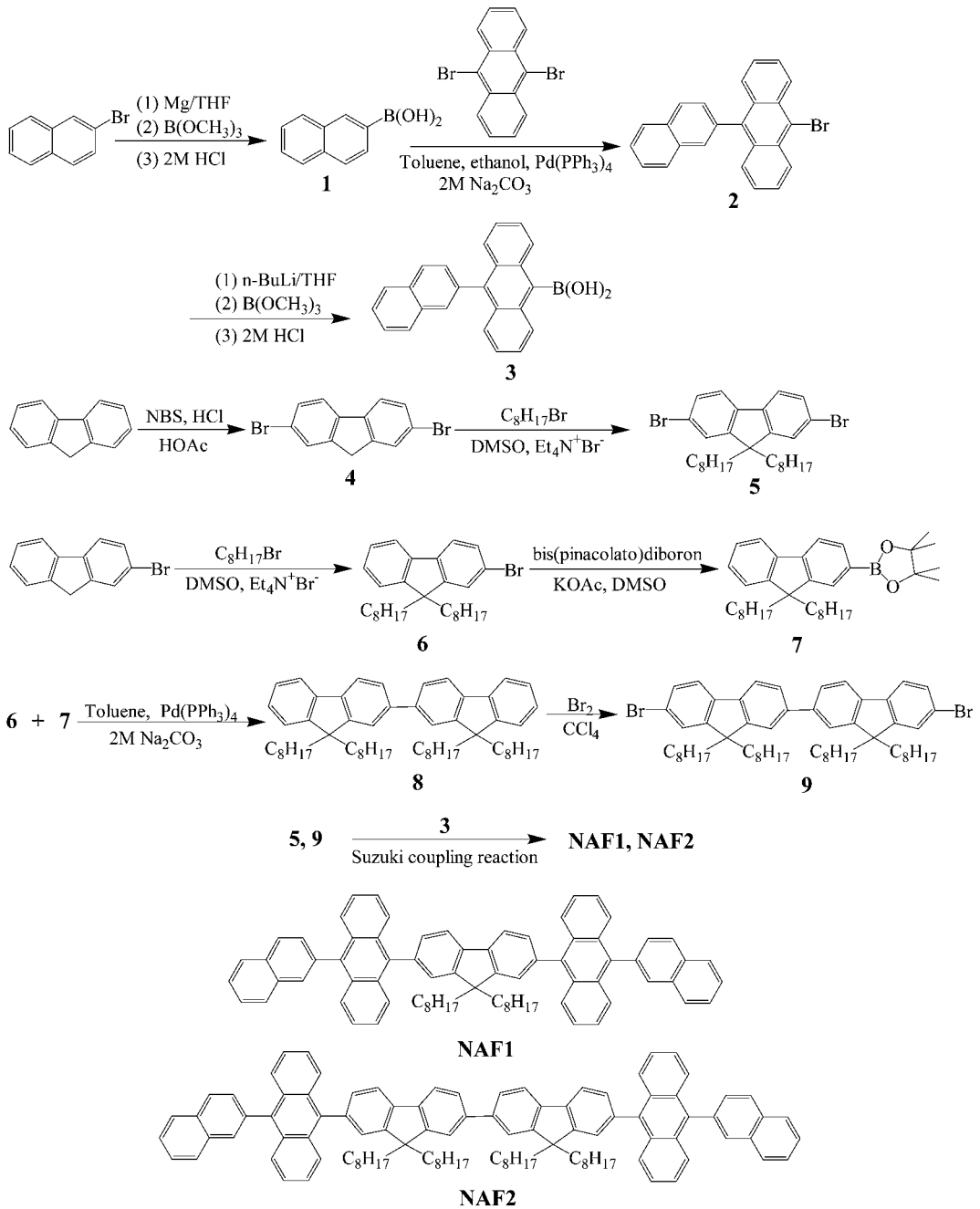

Scheme 1 Synthetic routes for **NAF1** and **NAF2**.

9-naphthylanthracene as the end caps at the C2 and C7 positions of fluorene to construct the first examples of fluorene/anthracene/naphthalene hybrids. Our results indicate the molecules designed in this way have non-planar structures, which are thus favorable to effectively inhibit self-aggregation and facilitates the formation of stable amorphous films.[21,22] Furthermore, these molecules are well soluble due to the non-planar conformation and the long alkyl substituents at the C9 position of fluorene moieties. The blue OLEDs containing **NAF1** or **NAF2** as a non-doped emitter show high efficiency of 4.02% (3.56 cd A^{-1} and 2.10 lm W^{-1}) with CIE coordinates of (0.15, 0.09). More importantly, these blue emitters serve as an efficient host for orange fluorescent dopant, and the two-emitting-component white OLEDs fabricated with **NAF1** host and an traditional orange dopant exhibited an efficiency of 7.66 cd A^{-1} with pure white color of (0.33, 0.33).

Experimental

General information

Chemicals, reagents and solvents from commercial sources are of analytical or spectroscopy grade and used as received without further purification. ^{1}H and ^{13}C NMR spectra were recorded on a Varian INOVA spectrometer (400 MHz). Mass spectra were recorded on a GC-Tof MS (Micromass, UK) mass spectrometer for TOF-MS-EI and a MALDI micro MX (Waters, USA) for MALDI-TOF-MS. Elemental analyses were carried out on a Carlo–Eriba 1106 elemental analyzer. Thermogravimetric analyses (TGA) and differential scanning calorimetry (DSC) measurements were performed on a Perkin-Elmer thermogravimeter (Model TGA7) and a Perkin-Elmer DSC 7 at a heating rate of 10 °C min^{-1} under a nitrogen atmosphere, respectively. The fluorescence and UV-vis absorption spectra measurements were performed on a Perkin-Elmer LS55 fluorescence spectrometer and a Perkin-Elmer Lambda 35 UV-Visible spectraphotometer, respectively. The phosphorescence quantum yields were determined against quinine sulfate as the standard ($\Phi = 0.55$ in water). Electrochemical measurements were made by using a conventional three-electrode configuration and an electrochemical workstation (BAS 100B, USA) at a scan rate of 100 mV s^{-1}. A glassy carbon working electrode, a Pt-wire counter electrode, and a saturated calomel electrode (SCE) as reference electrode were used. All measurements were made at room temperature on samples dissolved in dichloromethane, with 0.1 M tetra-*n*-butylammonium hexafluorophosphate (Bu_4NPF_6) as the electrolyte, ferrocene as the internal standard.

Device fabrication

The pre-cleaned ITO glass substrates (30 Ω $\square^{-1}$) were treated by UV-Ozone for 20 min. All the organic layers were deposited by vacuum evaporation in a vacuum chamber with a base pressure less than 10^{-6} torr. The cathode was completed through thermal deposition of LiF (1 nm) and then capping with Al metal (100 nm). The emitting area of each pixel is determined by overlapping of the two electrodes as 9 mm^2. The EL spectra, CIE coordinates, and current–voltage-luminance relationships of devices were measured with computer-controlled Spectrascan PR 705 photometer and a Keithley 236 source-measure-unit. All the measurements were carried out at room temperature under ambient conditions.

Compounds synthesis

The intermediates **1**, **2**, and **3**,[23–25] and **4**, **5**, **6**, **7**, and **8**,[26] were synthesized according to the literature methods.

7,7′-Dibromo-9,9,9′,9′-tetraoctyl-2,2′-bifluorene (9). Bromine (0.26 mL, 0.8 mmol) in CCl_4 (3 mL) was slowly added with stirring at 0 °C to a CCl_4 (15 mL) solution of the compound **8** (1 g, 1.28 mmol) containing a piece of iodine. The solution was stirred at 0 °C for 2 h in the dark, and 20 mL of aqueous $NaHCO_3$ (15%) was added. Vigorous stirring was applied until the red color disappeared. The organic layer was separated, washed with water and dried over anhydrous $MgSO_4$. The solvent was removed under vacuum and the residue was recrystallized from ethanol to give **9** as a white solid (1 g, 83% yield). Mp: 74.5–76.8 °C; ^{1}H NMR (400 MHz, $CDCl_3$, δ): 7.74 (d, J = 7.6 Hz, 2H; ArH), 7.63–7.57 (m, 6H; ArH), 7.48 (d, J = 8 Hz, 4H; ArH), 2.05–1.95 (m, 8H; CH_2), 1.21–1.08 (m, 40H; CH_2), 0.81 (t, J = 7.2 Hz, 12H; CH_3), 0.69 (m, 8H; CH_2).

2,7-Di(10-naphthylanthracene-9-yl)-9,9-dioctylfluorene (NAF1). A mixture of **3** (460 mg, 1.32 mmol), **5** (302 mg, 0.55 mmol) and Pd$(PPh_3)_4$ (63mg, 0.055 mmol) in toluene (15 mL) and 2 M aqueous Na_2CO_3 solution (2.8 mL, 5.5 mmol) was degassed by pump. The solution was heated at 80 °C for 18 h under argon. After the reaction mixture was cooled to room temperature, dichloromethane and water were added. The organic layer was separated and washed with diluted HCl and brine, then dried over anhydrous $MgSO_4$. The solvent was removed under vacuum and the residue was purified by column chromatography over silica gel with petroleum ether/CH_2Cl_2 (7 : 1) as the eluent to give **NAF1** as a light yellow solid (284 mg, 52% yield). ^{1}H NMR (400 MHz, $CDCl_3$, δ): 8.12–8.00 (m, 8H; ArH), 7.96 (d, J = 8 Hz, 2H; ArH), 7.89 (d, J = 8 Hz, 4H; ArH), 7.77 (d, J = 8 Hz, 4H; ArH), 7.67–7.56 (m, 10H; ArH), 7.40–7.33 (m, 8H; ArH), 2.09–2.05 (m, 4H; CH_2), 1.25–1.16 (m, 20H; CH_2), 0.99 (m, 4H; CH_2); 0.82 (t, J = 7.2 Hz, 6H; CH_3); ^{13}C NMR (400 MHz, $CDCl_3$, δ): 151.23, 140.46, 137.90, 136.91, 136.65, 133.46, 132.80, 130.28, 129.62, 128.14, 127.10, 126.47, 125.16, 119.83, 55.52, 40.52, 31.85, 30.11, 24.27, 22.62, 14.12; MALDI-TOF-MS (m/z): [M^+] calcd for $C_{77}H_{70}$, 994.5477; Found, 994.5214. Anal. calcd. for $C_{77}H_{70}$: C, 92.91; H, 7.09. Found: C, 92.64; H, 6.91.

7,7′-Di(10-naphthylanthracene-9-yl)-9,9,9′,9′-tetraoctyl-2,2′-bifluorene (NAF2). **NAF2** was prepared according to the method used for **NAF1** by using **3** (230 mg, 0.66 mmol), **9** (206 mg, 0.22 mmol) and Pd$(PPh_3)_4$ (26 mg, 0.022 mmol) in toluene (15 mL) and 2 M aqueous Na_2CO_3 solution (1.1 mL, 2.2 mmol). The crude product was purified by column chromatography over silica gel with petroleum ether/CH_2Cl_2 (6 : 1) as the eluent to give **NAF2** as a light yellow solid (122 mg, 40% yield). ^{1}H NMR (400 MHz, $CDCl_3$, δ): 8.11 (d, J = 8 Hz, 2H; ArH), 8.04–7.99 (m, 6H; ArH), 7.95 (d, J = 8 Hz, 4H; ArH), 7.87 (d, J = 8 Hz, 4H; ArH), 7.80–7.76 (m, 8H; ArH), 7.64–7.60 (m, 6H; ArH), 7.54–7.51 (m, 4H; ArH), 7.35–7.34 (m, 8H; ArH), 2.14–2.08 (m, 8H; CH_2),

1.25–1.16 (m, 40H; CH_2), 0.92–0.88 (m, 8H; CH_2); 0.82 (t, $J = 7.2$ Hz, 12H; CH_3); ^{13}C NMR (400 MHz, $CDCl_3$, δ): 152.01, 151.22, 140.45, 140.02, 137.69, 136.87, 136.66, 133.47, 132.80, 130.28, 129.62, 128.14, 127.11, 126.46, 125.15, 121.44, 120.10, 119.76, 55.48, 40.53, 31.95, 30.11, 24.13, 22.71, 14.10; MALDI-TOF-MS (m/z): [M^+] calcd for $C_{106}H_{110}$, 1382.8608; Found, 1383.5051. Anal. calcd. for $C_{106}H_{110}$: C, 91.99; H, 8.01. Found: C, 91.57; H, 7.69.

Results and discussion

Synthesis

The synthetic routes for the fluorene-cored derivatives with naphthylanthracene endcaps (**NAF1**, **NAF2**) are shown in Scheme 1. They were prepared by C–C coupling reaction of the boronic acid of the naphthylanthracene endcaps (**3**) and the bis-brominated oligo-fluorene core (**5** or **9**). First, the important intermediates for the synthesis of these target molecules, including 9-(2-naphthyl)anthracene-10-boronic acid (**3**),[23–25] 2,7-dibromo-9,9-dioctylfluorene (**5**) and 9,9,9′,9′-tetraoctyl-2,2′-bifluorene (**8**),[26] were synthesized according to literature methods, as described in Scheme 1. The 7,7′-dibromo-9,9,9′,9′-tetraoctyl-2,2′-bifluorene (**9**) was then obtained at a high yield of 83% by bromination of **8** in CCl_4 at low temperature of zero degree Celsius. It is found that use of the other solvents or increasing reaction temperature *e.g.* to room temperature or higher often resulted in tris-brominated byproducts. Finally the target compounds **NAF1** and **NAF2** were prepared at a moderate yield of 52% and 40% by Suzuki coupling reactions of the boronic acid **3** with the bis-brominated oligo-fluorene **5** and **9**, respectively. **NAF1** and **NAF2** have good solubility in common organic solvents so that they can be easily purified by column chromatography and recrystallization to high purity for spectroscopy characterization and OLEDs application. The chemical structures of **NAF1** and **NAF2** were confirmed by ^1H and ^{13}C NMR spectroscopy, matrix-assisted laser desorption ionization time-of-flight (MALDI-TOF) mass spectrometry, and elemental analysis. To the best of our knowledge, they are the first examples of fluorene/anthracene/naphthalene hybrids.

Thermal properties

The thermal properties of **NAF1** and **NAF2** were investigated by thermogravimetric analysis (TGA) and differential scanning calorimetry (DSC) at a scanning rate of 10 °C min^{-1} and the data are listed in Table 1. **NAF1** and **NAF2** exhibit high thermal stability with decomposition temperatures (T_d) up to 430 °C in N_2. The morphological stability of these molecules was monitored by the DSC measurements. As shown by the thermograms of **NAF1** in Fig. 1, only one endothermic peak due to melting was observed at 334 °C when a crystalline powder obtained from organic solvent is heated for the first run. The isotropic liquid would be rapidly self-cooled into the glassy state. In the second heating run, a glass transition was detected at 110 °C (T_g). Upon further heating beyond T_g, an exothermal peak was observed at 177 °C, which is ascribed to the crystallization. The melting is repeated when the temperature is increased to 334 °C. A glass transition temperature (T_g) of 110 °C indicates a relatively high amorphous stability of the **NAF1** solid films. We attribute the amorphous stability to the non-planar molecular structure of this molecule.[27] **NAF2** melted at 269 °C and no glass transition was observed under the present experimental condition. Based on the thermal and amorphous stability of these compounds, homogeneous and stable amorphous thin films of these compounds could be achieved by vacuum deposition, which matches the basic requirement for host emitters used in OLEDs.

Photophysical properties

The photophysical properties of **NAF1** and **NAF2** were investigated by means of electronic absorption and steady state photoluminescence (PL) spectra for both dilute solutions in dichloromethane and the solid films on quartz plates. The data are summarized in Table 1. Fig. 2 shows the absorption and PL spectra for **NAF1** as an example. The absorption spectrum of **NAF1** in dilute solution exhibits the characteristic vibrational

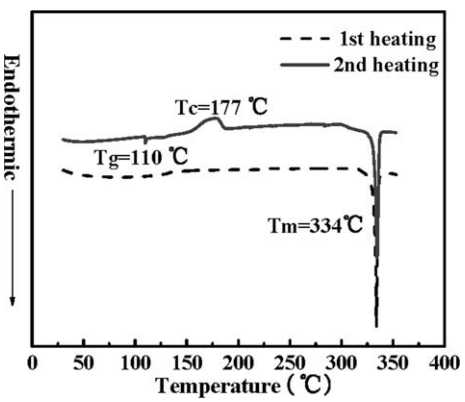

Fig. 1 DSC trace for **NAF1**. T_g: glass transition temperature; T_c: crystallization temperature; T_m: melting point.

Table 1 Summary of physical parameters of **NAF1** and **NAF2**

	λ_{max}^{abs} (nm)		λ_{max}^{em} (nm)									
Compound	CH_2Cl_2	Film	CH_2Cl_2	Film	Φ (%)[a]	T_g (°C)[b]	T_c (°C)	T_m (°C)	T_d (°C)	HOMO (eV)[c]	E_g (eV)[d]	LUMO (eV)
NAF1	399,379 360	403,383 361	436	444	70	110	177	334	438	−5.52	2.90	−2.62
NAF2	398,378 358,341	404,383 361,344	440	448	73	n.o.	133	269	430	−5.53	2.87	−2.66

[a] Measured in CH_2Cl_2 solution with quinine sulfate as the standard (Φ = 0.55 in water). [b] n.o. = not observed. [c] Calculated with reference to ferrocene (4.8 eV). [d] The energy band gap, calculated by the absorption edge technique.

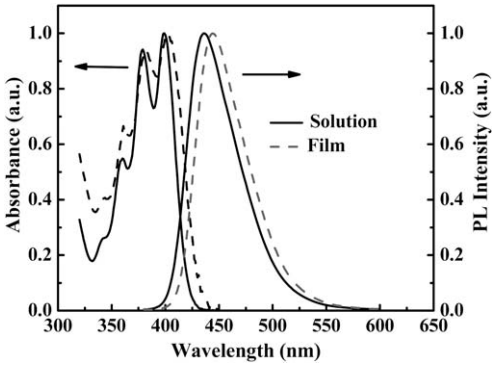

Fig. 2 Absorption and fluorescence spectra of **NAF1** in dilute dichloromethane solution and in solid film.

patterns of the isolated anthracene group with three bands at 399, 379 and 360 nm.[28] A red shift of 4 nm was detected in the absorption spectrum of **NAF1** thin film in comparison with that of the solution. Upon photoexcitation at the absorption maximum, the **NAF1** solution exhibits deep-blue fluorescence with emission peak at 436 nm. Similar to the absorption, a red shift of 8 nm was detected in the PL spectra of thin film. The absorption spectra of **NAF2** have similar features with those of **NAF1**, except with one additional band at 341 nm which should be ascribed to the π–π* transition of oligo-fluorene core. **NAF2** exhibits blue PL with emission peak at 440 nm in solution and 448 nm in thin film. The bathochromic effect in both absorption and PL spectra are frequently observed due to intermolecular interaction in solid state. However, the small red shift of only 4–8 nm in both absorption and PL spectra of present **NAF1** and **NAF2** reflects that the non-coplanar conformations of **NAF1** and **NAF2** molecules effectively inhibit unwanted intermolecular interaction and consequently guarantee the deep-blue emission color of these dyes in the solid state. The fluorescence quantum yield of **NAF1** and **NAF2** in dilute dichloromethane solution were determined as high as 70% and 73% when using quinine sulfate ($\Phi = 0.55$ in water) as the standard.[29] The high fluorescence quantum yield along with the agreeable emission color indicate that they may be used as efficient blue-light-emitting materials in OLEDs.

Electrochemical properties

Cyclic voltammetry (CV) measurements were performed using a conventional three-electrode cell set-up with 0.1 M tetra-*n*-butylammonium hexafluorophosphate (Bu_4NPF_6) as a supporting electrolyte in CH_2Cl_2, ferrocene as the internal standard, to investigate the electrochemical behaviors of these materials. The cyclovoltamograms are shown in Fig. 3. **NAF1** and **NAF2** show a reversible one-electron oxidation process with the onset potential of 0.72 and 0.73 V relative to ferrocene, respectively. The HOMO energy levels were estimated from the onset potentials to be 5.52 and 5.53 eV for **NAF1** and **NAF2** respectively, according to the equation of HOMO (eV) = $-(E_{ox}^{onset} + 4.8$ eV).[30] The energy band gaps were determined by the absorption edge technique.[30] The LUMO levels were calculated by subtracting the gap from the energy of the HOMO. The detailed electrochemical and electronic data of these two molecules are listed in Table 1.

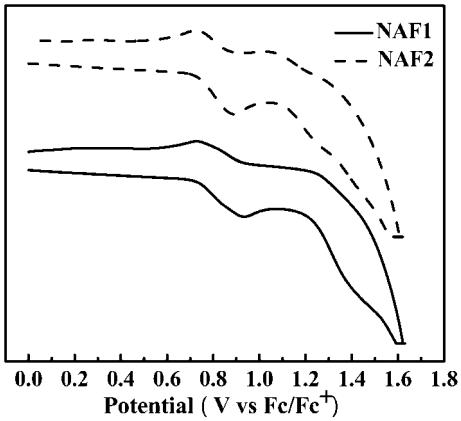

Fig. 3 Cyclic voltammograms of **NAF1** and **NAF2** measured in CH_2Cl_2 at a scan rate of 100 mV s^{-1}.

Electroluminescence of OLEDs

To investigate the electroluminescence (EL) properties of **NAF1** and **NAF2**, blue-emitting devices with a typical three-layer structure of ITO/NPB (40 nm)/**NAF1** (device I) or **NAF2** (device II) (15 nm)/TPBI (30 nm)/LiF (1 nm)/Al (200 nm) were fabricated. In these devices, NPB acts as the hole-transporting layer (HTL) and TPBI as the electron-transporting and hole-blocking layer (ETL), respectively. A 15 nm thick **NAF1** or **NAF2** film is deposited as the non-doped emitting layer (EML). Both device I and II exhibit deep-blue EL with emission peak at 448 nm and CIE coordinates of (0.15, 0.13) for **NAF1**, and 450 nm and CIE coordinates of (0.16, 0.13) for **NAF2**, as shown by the EL spectra in Fig. 4. The EL spectra and the CIE coordinates of these two OLEDs are observed to insensitive to the driving voltage, indicating a stable blue emission. The EL spectra show a small red shift of 2–4 nm compared with the PL of films. This is a frequently observed phenomena caused by the influence of the electrical field on the excited states in OLEDs.[31] As shown by the voltage-current density-luminance (*V*–*J*–*L*) characteristics and the efficiency curves in Fig. 5, the **NAF1** based device I exhibited a maximum brightness of 6528 cd m^{-2} at 8.5 V, and a maximum luminance efficiency (η_L) of 4.04 cd A^{-1} at 6 V, corresponding to a peak power efficiency (η_p) of 2.2 lm W^{-1} and an external quantum efficiency (η_{ext}) of 4.04%. The detailed performance of both device I and II are summarized in Table 2. Apparently, the

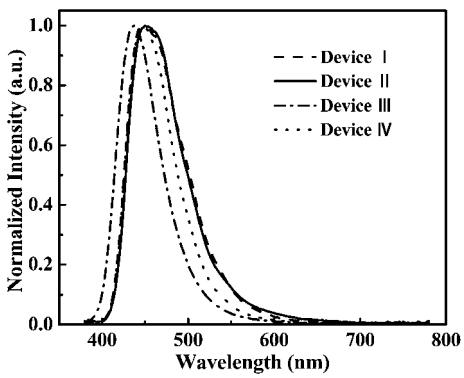

Fig. 4 EL spectra of blue devices I–IV.

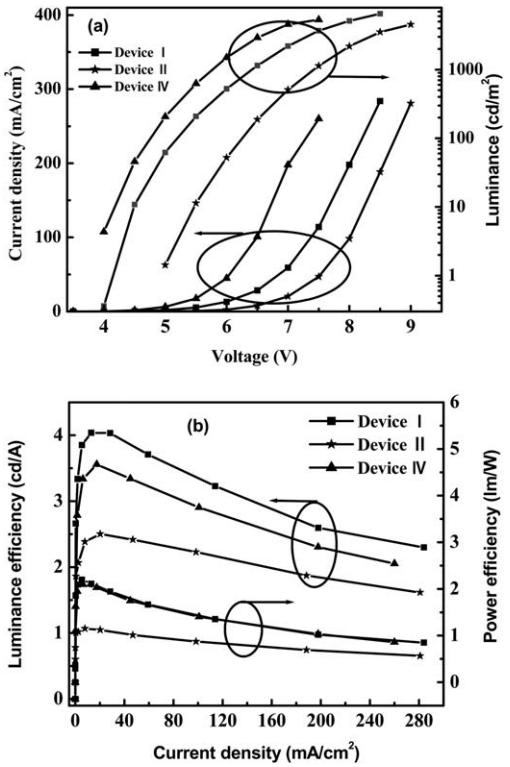

Fig. 5 (a) Voltage-current density-luminance (V–J–L) characteristics and (b) efficiencies curves for blue devices I, II and IV.

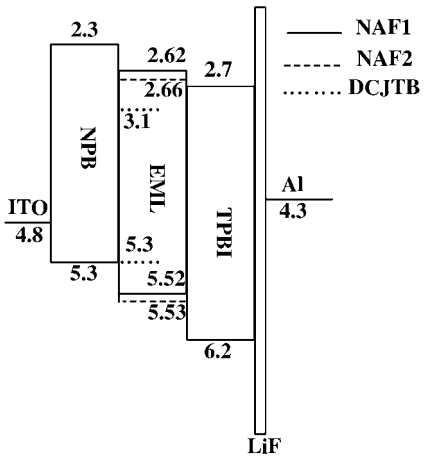

Fig. 6 Energy level diagrams for the OLEDs.

performances of **NAF1** based device I are among the best results ever reported for non-doped deep-blue OLEDs with CIE coordinate of $y \leq 0.15$. It should be noted that the overall performance of **NAF2** based device II are inferior to those of **NAF1** based device I, although the fluorescent quantum yield of **NAF2** is slightly higher. According to the energy levels diagrams for these two OLEDs in Fig. 6, both the hole injection barrier in NPB/EML interface (0.22 and 0.23 eV for **NAF1** and **NAF2**, respectively) and the electron injection barrier in TPBI/EML (0.08 and 0.04 eV for **NAF1** and **NAF2**, respectively) are both small enough to guarantee efficient hole and electron injection into the emitting layer in both devices. However, the current density at a given voltage in device II is much lower than that of device I (Fig. 5a). This probably results from the possible lower charge transporting mobility of **NAF2** film than **NAF1**.[32]

Since the hole transporting material NPB used in these devices is also a typical blue emitting material, it is necessary to verify the true origin of the deep-blue electroluminescence in these devices. For this purpose, we fabricate a reference device III with structure of ITO/NPB (55 nm)/TPBI (30 nm)/LiF (1 nm)/Al (200 nm), in which NPB acts as both hole transporting and emitting layer. The thickness of NPB layer in device III is controlled the same as the total of both HTL and EML in device I and II, to avoid any possible performance difference caused by different film thickness. The EL spectrum of device III is located at 438 nm, at least 10 nm shorter than those of device I and II. Furthermore, the luminance and efficiencies of the reference device III are quite lower than those of device I and II, as shown by the data in Table 2. All these results combine to confirm that EL in device I and II are indeed emitted by the **NAF1** and **NAF2** emitting layer, rather than from adjacent layers or interfaces.

In order to improve the performance of the blue emission, especially to obtain lower value of CIE coordinate y to approach the standard blue color, the thickness of NPB layer in device I was reduced to 30 nm, to obtain the device IV. Device IV exhibited lower turn-on voltage than device I due to the reduction in total thickness.[33] Furthermore, a narrowed EL spectrum (Fig. 4) and better CIE coordinates of (0.15, 0.09) were obtained. This CIE coordinates are quite close to the National Television System Committee (NTSC) standard blue of (0.14, 0.08). Although the emission efficiencies are slightly decreased as the expense in comparison with device I, a maximum luminance efficiency η_L of 3.56 cd A^{-1}, a maximum external quantum efficiency η_{ext} of 4.02% with an excellent CIE coordinates of (0.15, 0.09) for device IV (Fig. 5b and Table 2), are still among the best results ever reported for non-doped deep-blue OLEDs with a CIE coordinate of $y < 0.1$.

Table 2 Performance of devices I–VI

Device	$V_{turn\text{-}on}$ [V][a]	L_{max} (cd m^{-2}) ([b])	$\eta_{L(max)}$ (cd A^{-1}) ([b])	$\eta_{p(max)}$ (lm W^{-1}) ([b])	$\eta_{ext(max)}$ (%)[c]	λ_{max} (nm)	CIE (x, y)
I	4.1	6528 (8.5 V)	4.04 (6 V)	2.20 (5.5 V)	4.04	448	0.15,0.13
II	5	4541 (9 V)	2.50 (7 V)	1.15 (6.5 V)	2.50	450	0.16,0.13
III	3.5	2308 (7.5 V)	0.92 (5.5 V)	0.54 (5 V)	n.c.	438	0.15,0.07
IV	3.8	5339 (7.5 V)	3.56 (5.5 V)	2.10 (5 V)	4.02	448	0.15,0.09
V	6	20890 (15 V)	11.90 (13 V)	4.27 (6 V)	4.17 (13 V)	564	0.45,0.45
VI	5	12090 (12.5 V)	7.66 (10.5 V)	3.01 (6.5 V)	3.24 (10.5 V)	448, 556	0.33,0.33

[a] Recorded at 1 cd m^{-2}. [b] Values in the bracket are the voltages at which the data are obtained. [c] n.c = not calculated.

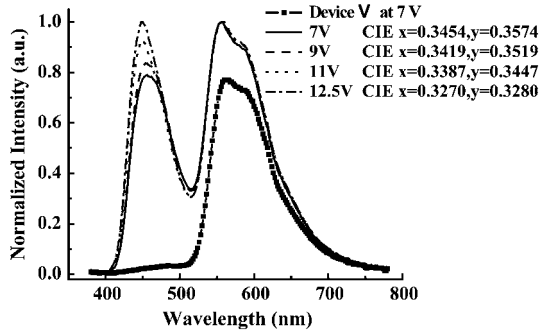

Fig. 7 EL spectra of orange device V (at 7 V) and white device VI (at various applied voltages).

The good performance of **NAF1** in the non-doped blue OLEDs prompts us to explore the possibility to use it as host emitter in host : dopant type of devices and finally to fabricate white OLEDs. For this purpose, a traditional yellow fluorophore, 4-(dicyanomethylene)-2-*tert*-butyl-6-(1,1,7,7-tetramethyljulolidyl-9-enyl)-4*H*-pyran (DCJTB), was selected as the yellow dopant to fabricate OLEDs with the following configuration: ITO/NPB (30 nm)/**NAF1**:DCJTB (1 : *x*) (30 nm)/TPBI (30 nm)/LiF (1 nm)/Al (200 nm) ($x = 2\%$: device V, $x = 0.2\%$: device VI). When the doping concentration is 2%, device V shows yellow emission (Fig. 7) from DCJTB with CIE coordinates of (0.45, 0.45), implying that efficient forward energy transfer from **NAF1** host to DCJTB can occur. This can be confirmed by the large spectral overlap between the absorption of DCJTB (spectrum not shown) and the fluorescence of **NAF1**. In addition, the HOMO and LUMO of DCJTB is located in between those of **NAF1** (shown in Fig. 6), implying that direct charge trapping by DCJTB combines with energy transfer to be responsible for the efficient EL of DCJTB in the doped OLEDs. When the doping concentration is reduced to 0.2%, device VI shows a balanced emission from both host and dopant as indicated by the EL spectra in Fig. 7. This two-emitting-component device exhibited a bright white light with CIE coordinates of (0.34, 0.35) at 7 V. With increasing the voltage, the color coordinates slightly shifted to (0.33, 0.33) at 12.5 V, which is just the standard white light of the National Television System Committee. The voltage-current density-luminance characteristics and the efficiency curves of the white OLED VI are illustrated in Fig. 8 and the data are listed in Table 2. The white OLED VI exhibited a maximum luminance (L_{max}) of 12 090 cdm^{-2} at 12.5 V. The maximum luminance efficiency reached to $\eta_L = 7.66$ cd A^{-1}, corresponding to a peak power efficiency of 3.01 lm W^{-1}. Although the efficiencies of our present white OLED are only close to the best data reported by Shu[17] for the two-emitting-component white OLEDs, the color coordinates of our device is superior to theirs over the whole detected voltage range. Most excitingly, the standard white light with (0.33, 0.33) is achieved for our **NAF1** based device at a high brightness over 10 000 cd m^{-2}.

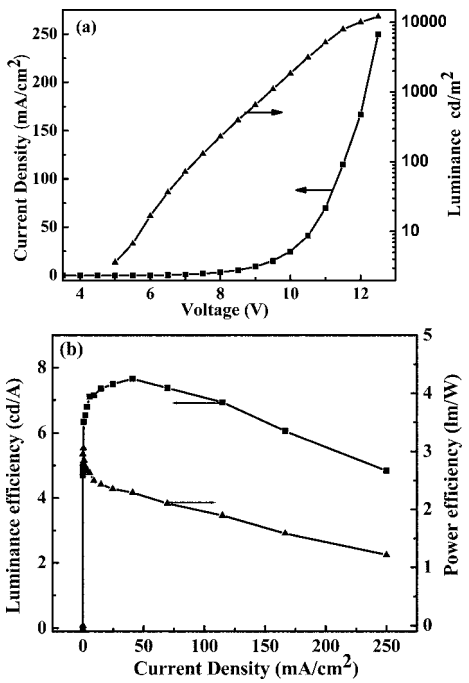

Fig. 8 (a) Voltage-current density-luminance (*V*–*J*–*L*) characteristics and (b) luminance efficiency and power efficiency as a function of current density for white device VI.

Conclusion

In summary, novel fluorene-cored deep-blue-emitting materials with naphthylanthracene endcaps, **NAF1** and **NAF2**, have been synthesized and investigated. A luminance efficiency of 3.56 cd A^{-1} (2.10 lm W^{-1} and 4.02%) and an almost standard blue coordinates (0.15, 0.09) were obtained in the non-doped OLEDs with **NAF1** as emitter, which is among the best performance ever reported for deep-blue OLEDs with a low CIE coordinate $y <$ 0.1. Furthermore, **NAF1** is capable of acting as host emitter in host : dopant emitting systems. The white OLEDs using **NAF1** as blue host and a traditional yellow fluorophore as dopant realized a high luminance of 12 090 cd m^{-2} and an efficiency of 7.66 cd A^{-1} with a standard white light coordinates of (0.33, 0.33), which is also among the best results ever reported for two-emitting-component white OLEDs based on fluorescent materials.

Acknowledgements

We thank the National Natural Science Foundation of China (U0634003, 20704002, 20923006, and 21072026), the Ministry of Education for the New Century Excellent Talents in University (Grant NCET-08-0074), the NKBRSF (2009CB220009), and the Fundamental Research Funds for the Central Universities (DUT10LK16) for financial support of this work.

References

1 C. W. Tang and S. A. Vanslyke, *Appl. Phys. Lett.*, 1987, **51**, 913.
2 L. S. Hung and C. H. Chen, *Mater. Sci. Eng., R*, 2002, **39**, 143.
3 L. M. Leung, W. Y. Lo, S. K. So, K. M. Lee and W. K. Choi, *J. Am. Chem. Soc.*, 2000, **122**, 5640.
4 S. Tang, M. Liu, P. Lu, H. Xia, M. Li, Z. Xie, F. Shen, C. Gu, H. Wang, B. Yang and Y. Ma, *Adv. Funct. Mater.*, 2007, **17**, 2869.
5 C.-H. Wu, C.-H. Chien, F.-M. Hsu, P.-I. Shih and C.-F. Shu, *J. Mater. Chem.*, 2009, **19**, 1464.
6 M. T. Lee, C. H. Liao, C. H. Tsai and C. H. Chen, *Adv. Mater.*, 2005, **17**, 2493.

7 C.-J. Zheng, W.-M. Zhao, Z.-Q. Wang, D. Huang, J. Ye, X.-M. Ou, X.-H. Zhang, C.-S. Lee and S.-T. Lee, *J. Mater. Chem.*, 2010, **20**, 1566.
8 Y.-H. Kim, D.-C. Shin, S.-H. Kim, C.-H. Ko, H.-S. Yu, Y.-S. Chae and S.-K. Kwon, *Adv. Mater.*, 2001, **13**, 1690.
9 Y. Tao, Q. Wang, Y. Shang, C. Yang, L. Ao, J. Qin, D. Ma and Z. Shuai, *Chem. Commun.*, 2009, 77.
10 C. H. Chuen, Y. T. Tao, F. I. Wu and C. F. Shu, *Appl. Phys. Lett.*, 2004, **85**, 4609.
11 C.-H. Chien, C.-K. Chen, F.-M. Hsu, C.-F. Shu, P.-T. Chou and C.-H. Lai, *Adv. Funct. Mater.*, 2009, **19**, 560.
12 J. Y. Li, D. Liu, C. Ma, O. Lengyel, C.-S. Lee, C.-H. Tung and S.-T. Lee, *Adv. Mater.*, 2004, **16**, 1538.
13 J. Y. Li and D. Liu, *J. Mater. Chem.*, 2009, **19**, 7584.
14 P. I. Shih, C. H. Chien, F. I. Wu and C. F. Shu, *Adv. Funct. Mater.*, 2007, **17**, 3514.
15 H. Sasabe, J. Takamatsu, T. Motoyama, S. Watanabe, G. Wagenblast, N. Langer, O. Molt, E. Fuchs, C. Lennartz and J. Kido, *Adv. Mater.*, 2010, **22**, 5003.
16 H. Wu, G. Zhou, J. Zou, C.-L. Ho, W.-Y. Wong, W. Yang, J. Peng and Y. Cao, *Adv. Mater.*, 2009, **21**, 4181.
17 P.-I. Shih, C.-Y. Chuang, C.-H. Chien, E. W.-G. Diau and C.-F. Shu, *Adv. Funct. Mater.*, 2007, **17**, 3141.
18 (*a*) J. Shi and C. W. Tang, *Appl. Phys. Lett.*, 2002, **80**, 3201; (*b*) Y.-H. Kim, H.-C. Jeong, S.-H. Kim, K. Yang and S.-K. Kwon, *Adv. Funct. Mater.*, 2005, **15**, 1799.
19 K. Kreger, M. Jandke and P. Strohriegl, *Synth. Met.*, 2001, **119**, 163.
20 Z. Q. Gao, Z. H. Li, P. F. Xia, M. S. Wong, K. W. Cheah and C. H. Chen, *Adv. Funct. Mater.*, 2007, **17**, 3194.
21 K. Danel, T. H. Huang, J. T. Lin, Y. T. Tao and C. H. Chuen, *Chem. Mater.*, 2002, **14**, 3860.
22 S. Wang, Jr, W. J. Oldham, Jr, R. A. Hudack and G. C. Bazan, *J. Am. Chem. Soc.*, 2000, **122**, 5695.
23 P. Wipf and J.-K. Jung, *J. Org. Chem.*, 2000, **65**, 6319.
24 S. L. Tao, Y. C. Zhou, C.-S. Lee, S.-T. Lee, D. Huang and X. H. Zhang, *J. Phys. Chem. C*, 2008, **112**, 14603.
25 L. Wang, W.-Y. Wong, M. F. Lin, W. K. Wong, K. W. Cheah, H. L. Tam and C. H. Chen, *J. Mater. Chem.*, 2008, **18**, 4528.
26 J. Jo, C. Y. Chi, S. Höger, G. Weger and D. Y. Yoon, *Chem.–Eur. J.*, 2004, **10**, 2681.
27 (*a*) J. Y. Li, C. Ma, J. Tang, C.-S. Lee and S. T. Lee, *Chem. Mater.*, 2005, **17**, 615; (*b*) S. B. Jiao, Y. Liao, X. J. Xu, L. P. Wang, G. Yu, L. M. Wang, Z. M. Su, S. H. Ye and Y. Q. Liu, *Adv. Funct. Mater.*, 2008, **18**, 2335.
28 *Handbook of Fluorescence Spectra of Aromatic Molecules*, ed. I. B. Berlman, Academic, New York, 2nd edn, 1971.
29 Z. J. Si, Y. Shao, C. X. Li and Q. Liu, *J. Lumin.*, 2007, **124**, 365.
30 D. Liu, H. C. Ren, J. Y. Li, Q. Tao and Z. X. Gao, *Chem. Phys. Lett.*, 2009, **482**, 72.
31 H. Yamamoto, J. Wilkinson, J. P. Long, K. Bussman, J. A. Christodoulides and Z. H. Kafafi, *Nano Lett.*, 2005, **5**, 2485.
32 Y.-H. Kim, H.-C. Jeong, S.-H. Kim, K. Y. Yang and S.-K. Kwon, *Adv. Funct. Mater.*, 2005, **15**, 1799.
33 E. L. Williams, K. Haavisto, J. Li and G. E. Jabbour, *Adv. Mater.*, 2007, **19**, 197.

